Phys Chem Minerals (2006) 32: 726–732
DOI 10.1007/s00269-005-0050-1

ORIGINAL PAPER

G. Diego Gatta · Yongjae Lee

On the elastic behaviour of zeolite mordenite: a synchrotron powder diffraction study

Received: 11 July 2005 / Accepted: 26 October 2005 / Published online: 24 November 2005

Abstract The high-pressure elastic behaviour of a synthetic zeolite mordenite, $Na_6Al_{6.02}Si_{42.02}O_{96}\cdot 19H_2O$ [$a = 18.131(2)$, $b = 20.507(2)$, $c = 7.5221(5)$ Å, space group $Cmc2_1$], has been investigated by means of in situ synchrotron X-ray powder diffraction up to 5.68 GPa. No phase transition has been observed within the pressure range investigated. Axial and volume bulk moduli have been calculated using a truncated second-order Birch–Murnaghan equation-of-state (II-BM-EoS). The refined elastic parameters are: $V_0 = 2801(11)$ Å^3, $K_{T0} = 41(2)$ GPa for the unit-cell volume; $a_0 = 18.138(32)$ Å, $K_{T0}(a) = 70(8)$ GPa for the *a*-axis; $b_0 = 20.517(35)$ Å, $K_{T0}(b) = 29(2)$ GPa for the *b*-axis and $c_0 = 7.531(5)$ Å, $K_{T0}(c) = 38(1)$ GPa for the *c*-axis [$K_{T0}(a)$: $K_{T0}(b)$: $K_{T0}(c) = 2.41{:}1.00{:}1.31$]. Axial and volume Eulerian finite strain versus "normalized stress" plots (*fe–Fe* plot) show an almost linear trend and the weighted linear regression through the data points yields the following intercept values: $Fe(0) = 39(4)$ GPa for *V*; $Fe_a(0) = 65(18)$ GPa for *a*; $Fe_b(0) = 28(3)$ GPa for *b*; $Fe_c(0) = 38(2)$ GPa for *c*. The magnitudes of the principal Lagrangian unit-strain coefficients, between 0.47 GPa (the lowest H*P*-data point) and each measured $P > 0.47$ GPa, were calculated. The unit-strain ellipsoid is oriented with $\varepsilon_1 \parallel b$, $\varepsilon_2 \parallel c$, $\varepsilon_3 \parallel a$ and $|\varepsilon_1| > |\varepsilon_2| > |\varepsilon_3|$. Between 0.47 and 5.68 GPa the relationship between the unit-strain coefficient is $\varepsilon_1{:}\ \varepsilon_2{:}\ \varepsilon_3 = 2.16{:}1.81{:}1.00$. The reasons of the elastic anisotropy are discussed.

Keywords Zeolite · Mordenite · High-pressure · Synchrotron X-ray powder diffraction · Compressibility

G. D. Gatta (✉)
Dipartimento di Scienze della Terra, Università degli Studi di Milano, Via Botticelli 23, I-20133 Milano, Italy
E-mail: diego.gatta@unimi.it
Tel.: +39-02-50315607
Fax: +39-02-50315597

Y. Lee
Department of Earth System Sciences, Yonsei University, 120749 Seoul, Korea

Introduction

Mordenite is a natural zeolite found in vugs of volcanic and intrusive igneous rocks or as a diagenetic product of volcanic tuff, with ideal composition: $(Na_2,K_2,Ca)_4[Al_8Si_{40}O_{96}]\cdot 28H_2O$ (Gottardi and Galli 1985; Armbruster and Gunter 2001; Passaglia and Sheppard 2001). The crystal structure was first described in the space group *Cmcm* (Meier 1961). Further investigations showed that, even though the topological symmetry is *Cmcm*, the general symmetry of mordenite is $Cmc2_1$ (Alberti et al. 1986; Simoncic and Armbruster 2004). The lowering of symmetry to the acentric group (from *Cmcm* to $Cmc2_1$) appears necessary to avoid an energetically unfavourable T-O-T angle of 180° in *Cmcm*. In addition, Alberti et al. (1986) showed that also the topological configuration of the extra-framework content conforms to $Cmc2_1$. The crystal structure of mordenite is built by layers formed of six-membered rings parallel to (100) (Fig. 1a) which are connected by four-membered ring to form a 3D-framework. One secondary building unit (SBU) can be found: the 5-1 SBU (Baerlocher et al. 2001). The tetrahedral framework of mordenite shows three different systems of channels. Two systems parallel to [001]: a 12-membered ring channel (12mR[001], with "free diameters" 6.5×7.0 Å, Baerlocher et al. 2001) and a strongly elliptic ("compressed") eight-membered ring channel (8mR[001], "free diameters" 2.6×5.7 Å) (Fig. 1b). The 12mR[001] and 8mR[001] channels are connected by eight-membered double rings parallel to [010], which form the third channels system (8mR[010], "free diameters" 3.4×4.8 Å)(Fig. 1b). The "framework density" of mordenite (defined as the number of tetrahedrally co-ordinated atoms, T-atoms, per 1,000 Å^3) is: 17.2 T/1,000 Å^3 (Baerlocher et al. 2001).

The high-temperature (H*T*) behaviour of mineral and synthetic mordenites have been investigated by several authors by means of thermogravimetric analysis, in situ and *ex situ* H*T*-single crystal X-ray diffraction and in situ

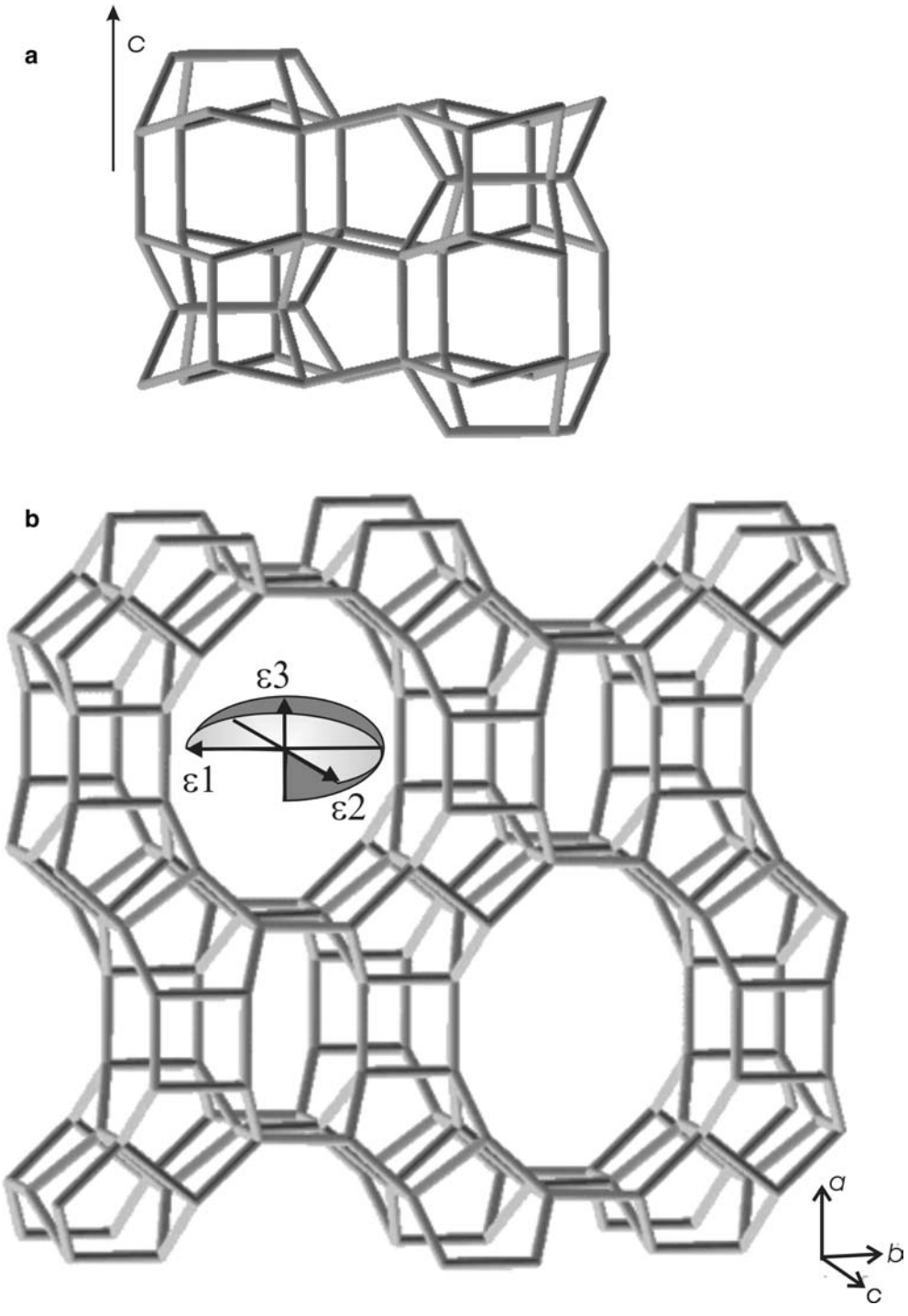

Fig. 1 Skeletal representation of the mordenite framework: **a** six-membered ring parallel to (100), **b** clinographic view showing the three channel systems (12mR[001], 8mR[001] and 8mR[010]) and the orientation of the unit-strain ellipsoid

time resolved H*T*-synchrotron X-ray powder diffraction (Mortier et al. 1975, 1976; Schlenker et al. 1978a, b, c, 1979; Gottardi and Galli 1985; Elsen et al. 1987; Bish and Carey 2001; Martucci et al. 2003). Martucci et al. (2003), on the basis of H*T*-synchrotron X-ray powder diffraction data between 23 and 830°C, showed the main deformation mechanisms and the continuous structural transformation of a natural mordenite upon complete dehydration, which occur at about 800°C. A slight reduction of the cell-volume within the *T*-range investigated was observed (-1.9%). The structural refinements showed that during dehydration the extra-framework content migrates to new sites, in order to achieve a new configuration being energetically favourable. In addition, the main deformation mechanism, which acts on the Si/Al-framework is the change in ellipticity of the 8mR[010] as a result of dehydration and cation migration toward the channel walls.

Whereas a large number of studies have been devoted to the H*T*-behaviour of natural or cation-exchanged mordenites, no elastic data are available. The aim of this study is to investigate the high-pressure behaviour (H*P*) of mordenite under hydrostatic conditions by means of in situ synchrotron X-ray powder diffraction. The small dimensions and the quality of natural or synthetic crystals hinder any H*P* single-crystal diffraction study.

Experimental methods

A synthethic sample of mordenite with composition $Na_6Al_{6.02}Si_{42.02}O_{96}{\cdot}19H_2O$ ($a = 18.131(2)$, $b = 20.507(2)$, $c = 7.5221(5)$ Å, space group $Cmc2_1$) for the H*P*-experiments was kindly provided by Petra Simoncic. The structural refinement of this synthetic mordenite was performed on the basis of synchrotron X-ray single-crystal diffraction data. Further details are in Simoncic and Armbruster (2004).

In situ H*P* synchrotron X-ray powder diffraction experiments were performed at the X7A beamline at the national synchrotron light source (NSLS) at brookhaven national laboratory (BNL). The primary white beam from the bending magnet was focused in the horizontal plane by a triangular Si (111) monochromator bent to a cylindrical curvature by applying a load to the crystal tip, creating ~200 μm focused monochromatic radiation of ~0.7 Å (Lemonnier et al. 1978). A tungsten wire crosshair was positioned at the centre of the goniometer circle and subsequently the position of the incident beam was adjusted to the crosshair. A gas-proportional position-sensitive detector (Smith 1991) covering 4° in 2θ was stepped in 0.25° intervals over the angular range of 3–20° with counting times of 90–150 s per step. The wavelength of the incident beam was 0.6232(1) Å as determined from a CeO_2 standard (SRM 674).

A modified Merrill–Bassett diamond anvil cell (DAC) was used for the H*P*-experiments, equipped with two type-I diamonds anvils (Miletich et al. 2000) (culet face diameter: 500 μm) and tungsten-carbide supports. Stainless-steel foil, 250 μm thick, pre-indented to a thickness of about 100 μm, with a 200 μm hole obtained by electro-spark erosion, was used as a gasket. A powdered sample of mordenite was placed in the gasket hole together with some ruby chips for the pressure measurements. The pressure at the sample was measured by detecting the shift in the R1 emission line of the included ruby chips according to the Forman et al. (1972) and Mao et al. (1986) (precision: ± 0.1 GPa). A methanol:ethanol:water (16:3:1) mixture was used as hydrostatic pressure-transmitting medium (Hazen and Finger 1982; Miletich et al. 2000). The sample was equilibrated for about 60 min at each measured pressure and after the diffraction data measurement the pressure was raised by ~0.5 GPa increments. However, the measured diffraction data suffered from sample texture effects and showed some broadening of the peaks at $P > 3$–4 GPa. Unit cell constants were determined by LeBail whole pattern fitting using the GSAS package (LeBail et al. 1988; Larson and Von Dreele 2004) up to 5.68 GPa (Table 1). The background curve was fitted with a Chebyshev polynomial with six coefficients. The pseudo-Voigt profile function proposed by Thomson et al. (1987) was used to fit the experimental pattern. The diffraction peaks were modelled by varying only the half-width parameter in the pseudo-Voigt profile function. Due to the quality of the H*P*-diffraction patterns and to the large number of the independent parameters of the crystal structure of mordenite, any attempt of structural refinement by Rietveld method (Rietveld 1969) was unsuccessful.

Results: elastic parameters of mordenite

The unit-cell parameters of mordenite measured at different pressures are reported in Table 1 and their H*P*-evolution is shown in Fig. 2. Unit-cell volume data were fitted with a truncated II-BM-EoS (Birch 1947; Angel 2000) using the EOS-FIT5.2 program (Angel 2001). The BM-EoS parameters, simultaneously refined using the data weighted by the uncertainties in P and V, are: $V_0 = 2801(11)$ Å^3, $K_{T0} = 41(2)$ GPa and $K' = 4.0$ (fixed).

The "axial bulk moduli" were calculated with a "linearized" II-BM-EoS (Angel 2000), substituting the cube of the individual lattice parameter (a^3, b^3 and c^3) for the volume. The axial-EoS parameters, refined using the data weighted by the uncertainties in P and a^3, b^3, c^3, are: $a_0 = 18.138(32)$ Å, $K_{T0}(a) = 70(8)$ GPa [$\beta_a = 0.014(2)$ GPa^{-1}] for the a-axis; $b_0 = 20.517(35)$ Å, $K_{T0}(b) = 29(2)$ GPa [$\beta_b = 0.034(3)$ GPa^{-1}] for the b-axis and $c_0 = 7.531(5)$ Å, $K_{T0}(c) = 38(1)$ GPa [$\beta_c = 0.026(1)$ GPa^{-1}] for the c-axis. The high *e.s.d.* of the a_0, b_0 and V_0 value is due to the absences of the experimental data in DAC under room conditions. The linearized bulk moduli show a strong anisotropic elastic behaviour of this zeolite along the three mutually perpendiculars directions parallel to [100], [010] and [001], being $K_{T0}(a)$: $K_{T0}(b)$: $K_{T0}(c) = 2.41{:}1.00{:}1.31$.

Axial and volume Eulerian-finite strain ($f_e = [(V_0/V)^{2/3}-1]/2$) vs. "normalized stress" ($F_e = P/[3f_e(1+2f_e)^{5/2}]$) plots (*fe–Fe* plot; Angel 2000) are shown in Fig. 3. The weighted linear regression through the data points yields the following intercept values: $Fe_a(0) = 65(18)$ GPa for the a-axis; $Fe_b(0) = 28(3)$ GPa for the b-axis; $Fe_c(0) = 38(2)$ GPa for the c-axis; $Fe_V(0) = 39(4)$ GPa for the unit-cell volume. The slope of the regression lines is almost horizontal and justify the use of the truncated II-BM-EoS for the axial and volume bulk moduli calculation. In addition, the normalized stress values obtained at $fe = 0$ [i.e. $Fe_a(0)$, $Fe_b(0)$, $Fe_c(0)$ and $Fe_V(0)$], show a good agreement with the axial and volume bulk moduli obtained by the EoS-fit [i.e. K_{T0}, $K_{T0}(a)$, $K_{T0}(b)$ and $K_{T0}(c)$].

The magnitudes of the principal Lagrangian unit-strain coefficients, between 0.47 GPa (the lowest H*P*-data point) and each measured $P > 0.47$ GPa, were

Table 1 Lattice parameters of mordenite and full-profile fit agreement parameters (Rp, χ^2) at different pressures

P (GPa)[a]	a (Å)	b (Å)	c (Å)	V (Å^3)	Rp	χ^2
0.47	18.106(3)	20.415(3)	7.5019(9)	2772.9(5)	0.1306	6.655
1.35	18.023(3)	20.227(2)	7.4479(6)	2715.2(4)	0.0880	7.565
2.71	17.927(3)	20.002(2)	7.3782(8)	2645.6(5)	0.1137	4.694
3.90	17.796(2)	19.752(2)	7.3126(7)	2570.3(4)	0.0702	4.469
4.48	17.786(3)	19.700(3)	7.2914(9)	2554.8(6)	0.0894	5.535
5.68	17.760(7)	19.573(4)	7.243(2)	2517.9(13)	0.0642	3.755

[a] *e.s.d.* ± 0.1 GPa

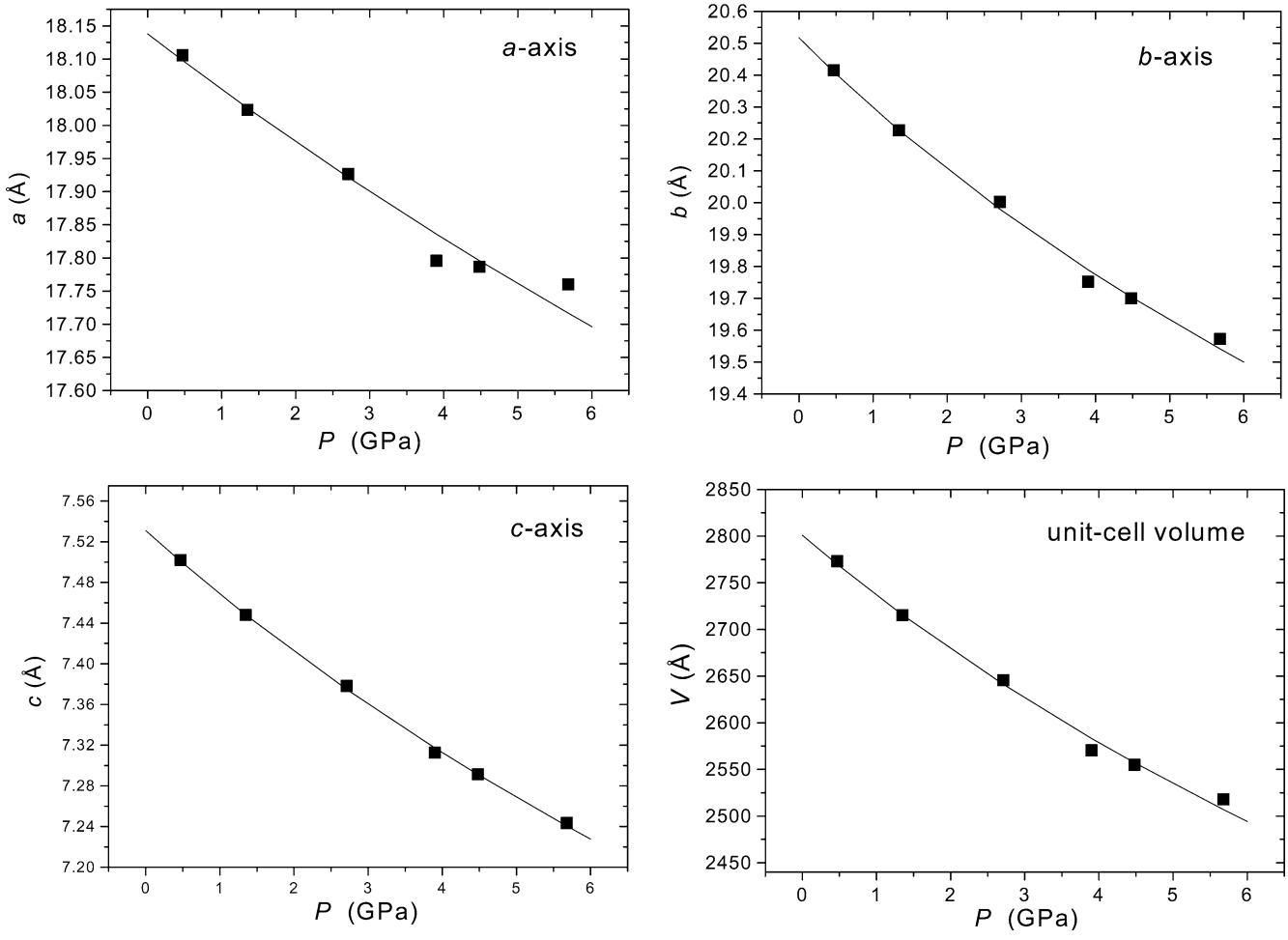

Fig. 2 Evolution of the unit-cell parameters of mordenite with pressure. The *esds* values are smaller than the size of the symbols. *Solid lines* represent the axial and volume fit with a II-BM-EoS

calculated with the STRAIN software (Ohashi 1982) (Table 2). The unit-strain ellipsoid is oriented with $\varepsilon_1 \parallel b$, $\varepsilon_2 \parallel c$, $\varepsilon_3 \parallel a$ with $|\varepsilon_1| > |\varepsilon_2| > |\varepsilon_3|$, as shown in Fig. 1b. The evolution of the unit-strain coefficients with pressure is shown in Fig. 4. The magnitude of all three unit-strain coefficients decreases slightly with P, following a linear behaviour. Whereas the slopes of ε_3 and ε_2 versus P appear to be almost parallel, the slope of ε_1 is slightly higher, implying a possible convergence to ε_2 at $P > 6$ GPa (Fig. 4). Between 0.47 and 5.68 GPa we have ε_1: ε_2: $\varepsilon_3 = 2.16{:}1.81{:}1.00$.

On the basis of the *fe–Fe* plots and of the unit-strain coefficients behaviour we can prudently infer that no phase transition occurs within the P-range investigated. However, the axial EoS-fit shows that at $P > 3$ GPa the a-values slightly misfit the theoretical EoS curve, but this behaviour is not observed for the other unit-cell constants. We cannot exclude, therefore, that there is a slight change on the compressional behaviour at $P > 3$ GPa [with an increase in $K_{T0}(a)$], as well as we cannot exclude that the slight misfit for the a-EoS is due to the low quality of the diffraction data at $P > 3$ GPa,

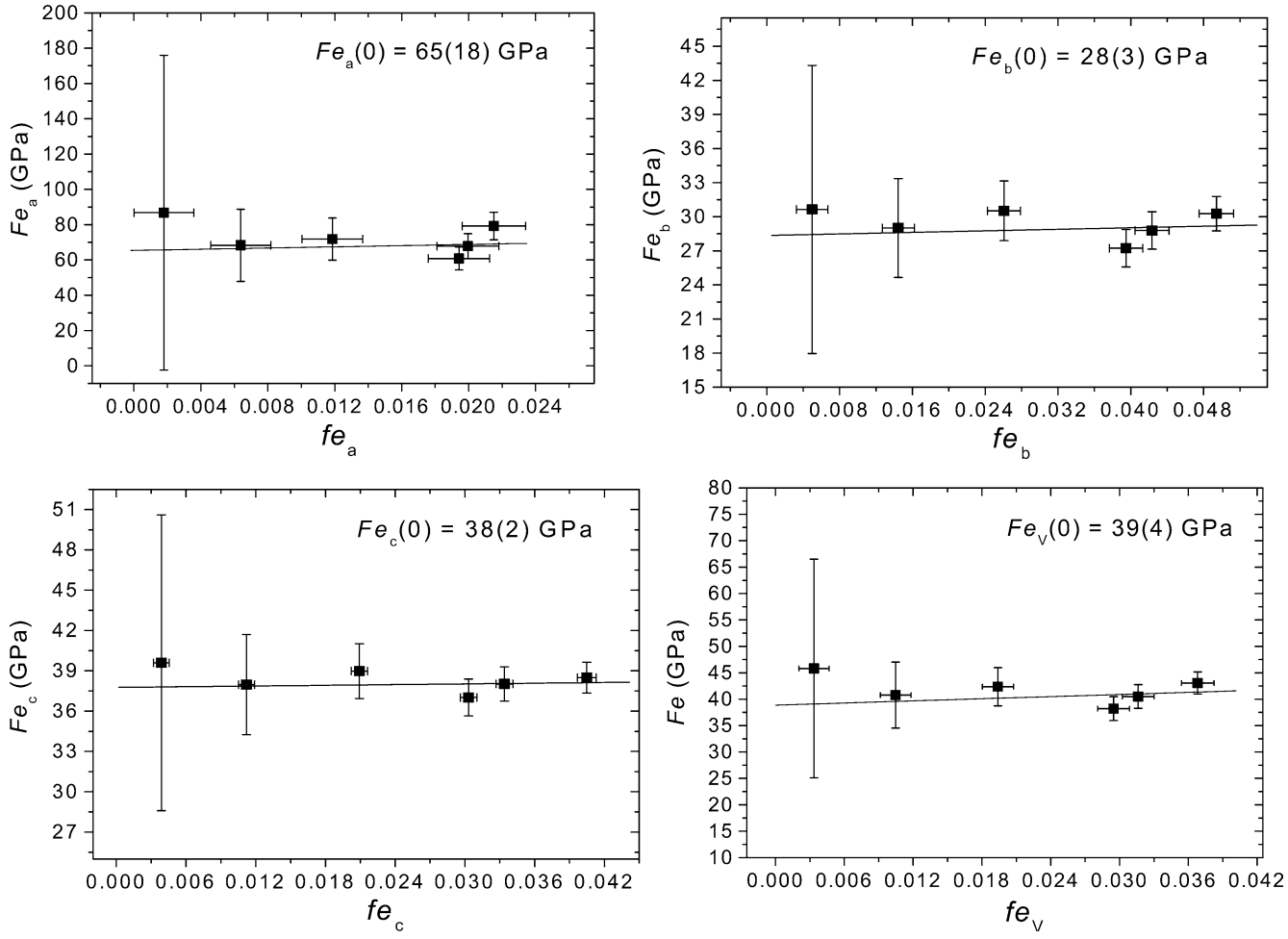

Fig. 3 Axial and volume *fe–Fe* plots. The *esds* were calculated according to Heinz and Jeanloz (1984). The solid lines are the weighted linear fit through the data

which hinders any accurate lattice parameters determination.

Discussion and conclusion

Mordenite is the first zeolite with MOR topology (Baerlocher et al. 2001) investigated under *P*. Only bikitaite, a lithium zeolite (BIK topology), which shows some affinity with the MOR topology (Gottardi and Galli 1985), was already investigated under *P* by means of single-crystal diffraction (Comodi et al. 2003) and synchrotron powder diffraction (Ferro et al. 2002). The bulk modulus of mordenite obtained in this study [$K_{T0} = 41(2)$ GPa] is close to the bulk modulus of bikitaite [K_{T0}(bikitaite) = 44.2(4) GPa, Comodi et al. 2003; K_{T0}(bikitaite) = 45(1) GPa, Ferro et al. 2002], slightly lower then that of the "fibrous zeolites group" (average bulk modulus $K_{T0} = 50 \pm 10$ GPa, Gatta 2005 and references therein) and higher then zeolites with similar large channel [K_{T0} (heulandite) = 27.5(2) GPa, Comodi et al. 2001). The axial bulk moduli show that under pressure the crystal structure of mordenite responds with a strong anisotropic elastic behaviour, being $K_{T0}(a) > K_{T0}(c) > K_{T0}(b)$. This behaviour is confirmed by the magnitude of unit-strain coefficients.

The reasons for the observed anisotropic compression can be intuitively assumed on the basis of the crystal structure of mordenite and on the basis of the H*T*-structural behaviour. The ellipticity of both 12mR[001] and 8mR[001] channels is given by the major axis parallel to [100] (Fig. 1b). This implies that any *P*-induced compression along [100] leads to a drastic change in the configuration of the aforementioned channels, which is energetically unfavourable. It is more likely that under hydrostatic-*P* the structure reacts with a strong shortening along [010] then along [100], maintaining the original elliptical configuration of the 12mR[001] and 8mR[001]. Although, the crystal structure of mordenite appears to be more compact along [001] than along [100] or [010], the H*T*-study demonstrated that the framework is "flexible" along [001]. In fact, Martucci et al. (2003) reported that the main deformation mechanism of the tetrahedral framework at

Table 2 Magnitude of the principal Lagrangian unit-strain coefficients (between 0.47 GPa and *P*) and orientation of the unit-strain ellipsoid at high-pressure

ΔP (GPa)	$\lvert\varepsilon_1\rvert$ (GPa^{-1})	$\lvert\varepsilon_2\rvert$ (GPa^{-1})	$\lvert\varepsilon_3\rvert$ (GPa^{-1})
1.35–0.47	0.0105(2)	0.0082(1)	0.0051(2)
2.71–0.47	0.0090(3)	0.0074(2)	0.0044(3)
3.90–0.47	0.0095(3)	0.0074(2)	0.0050(3)
4.48–0.47	0.0087(3)	0.0070(2)	0.0044(3)
5.68–0.47	0.0079(3)	0.0066(2)	0.0037(4)

Note: $\varepsilon_1 \parallel b$, $\varepsilon_2 \parallel c$, $\varepsilon_3 \parallel a$

H*T* is the enlargement of the 8mR[010], due to the flattening of some T-O-T angles. This mechanism implies changes on the configuration of the 8mR[010] mainly along [100] and [001]. We can assume, therefore, that under *P*-condition the 8mR[010] channels are compressed more along [001] than along [100], in order to maintain the original configuration (i.e. without any "inversion" in ellipticity, Fig. 1b). The aforementioned mechanisms reasonably explain the reasons of the elastic anisotropy of mordenite and appear to confirm a general principle concerning the H*P*-behaviour of microporous materials: the open framework structures tend to accommodate the effect of pressure, by cooperative rotation of the tetrahedra, *usually* increasing the ellipticity of the channel systems and maintaining the original elliptical configuration, without any "inversion" in ellipticity (Ballone et al. 2002; Comodi et al. 2002; Gatta and Wells 2004; Gatta et al. 2003, 2004a, b; Lee et al. 2002a, b, 2004). In this context, the anisotropic behaviour of mordenite, and of other open framework compounds not investigated under pressure, can be intuitively expected. In reality, however, the bonding between the host zeolitic framework and the stuffed guest species would also affect the overall compression behaviour (Fois et al. 2005) and it would be interesting to investigate such effects.

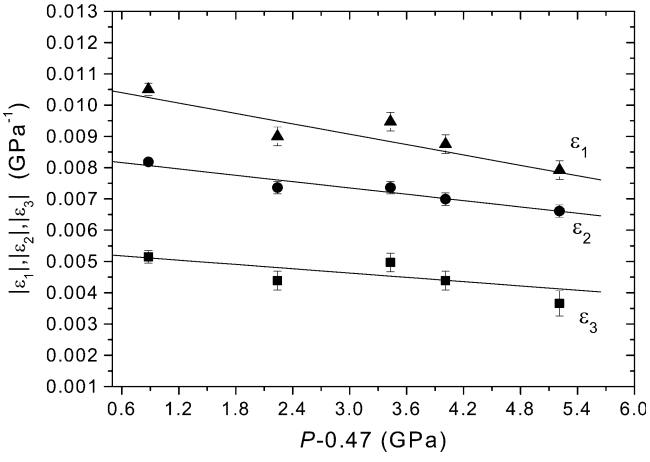

Fig. 4 Magnitude of the principal Lagrangian unit-strain coefficients calculated between 0.47 GPa and *P*. The lines are the weighted linear fit through the data

Acknowledgements The graphical representations of the mordenite structure are from Ch. Baerlocher and L.B. McCusker, Database of Zeolite Structures: http://www.iza-structure.org/databases/. Research carried out in part at the NSLS at BNL is supported by the U.S. DOE (DE-Ac02-98CH10886 for beam line X7A). A special thanks is due to Petra Simoncic for the sample of synthetic mordenite. The editor M. Rieder, M. Gunter and an anonymous referee and N. Rotiroti are thanked for their helpful suggestions.

References

Alberti A, Davoli P, Vezzalini G (1986) The crystal structure refinement of a natural mordenite. Z Kristallogr 175:249–256

Angel RJ (2000) Equation of state. In: Hazen RM, Downs RT (eds) High-temperature and high-pressure crystal chemistry. Reviews in mineralogy and geochemistry, vol 41. Mineralogical Society of America and Geochemical Society, Washington, DC, pp 35–59

Angel RJ (2001) EOS-FIT V6.0. Computer program. Crystallography laboratory, department geological sciences, Virginia Tech, Blacksburg, USA

Armbruster T, Gunter ME (2001) Crystal structures of natural zeolites. In: Bish DL, Ming DW (eds) Natural zeolites: occurrence, properties, application. Reviews in mineralogy and geochemistry, vol 45. Mineralogical Society of America and Geochemical Society, Washington, DC, pp 1–57

Baerlocher CH, Meier WM, Olson DH (2001) Atlas of zeolite framework types, 5th edn. Elsevier, Amsterdam, NL, p 302

Ballone P, Quartieri S, Sani A, Vezzalini G (2002) High-pressure deformation mechanism in scolecite: a combined computational-experimental study. Am Miner 87:1194–1206

Bish DL, Carey JW (2001) Thermal properties of natural zeolites. In: Bish DL, Ming DW (eds) Natural zeolites: occurrence, properties, application. Reviews in mineralogy and geochemistry, vol 45. Mineralogical Society of America and Geochemical Society, Washington, DC, pp 403–452

Birch F (1947) Finite elastic strain of cubic crystal. Phys Rev 71:809–824

Comodi P, Gatta GD, Zanazzi PF (2001) High-pressure structural behaviour of heulandite. Eur J Miner 13:497–505

Comodi P, Gatta GD, Zanazzi PF (2002) High-pressure behaviour of scolecite. Eur J Miner 14:567–574

Comodi P, Gatta GD, Zanazzi PF (2003) Effects of pressure on the structure of bikitaite. Eur J Miner 15:247–255

Elsen J, King GSD, Mortier WJ (1987) Influence of temperature on the cation distribution in calcium mordenite. J Phys Chem 91:5800–5805

Ferro O, Quartieri S, Vezzalini G, Fois E, Gamba A, Tabacchi G (2002) High-pressure behaviour of bikitaite: an integrated theoretical and experimental approach. Am Miner 87:1415–1425

Fois E, Gamba A, Tabacchi G, Arletti R, Quartieri S, Vezzalini G (2005) The "template" effect of the extra-framework content on zeolite compression: the case of yugawaralite. Am Miner 90:28–35

Forman RA, Piermarini GJ, Barnett JD, Block S (1972) Pressure measurement made by utilisation of ruby sharp-line luminescence. Science 176:284–286

Gatta GD (2005) A comparative study of fibrous zeolites under pressure. Eur J Miner 17:411–422

Gatta GD, Wells SA (2004) Rigid unit modes at high-pressure: an explorative study of a fibrous zeolite like framework with EDI topology. Phys Chem Miner 31:465–474

Gatta GD, Comodi P, Zanazzi PF (2003) New insights on high-pressure behaviour of microporous materials from X-ray single-crystal data. Micr Mesop Mat 61:105–115

Gatta GD, Boffa Ballaran T, Comodi P, Zanazzi PF (2004a) Isothermal equation of state and compressional behaviour of tetragonal edingtonite. Am Miner 89:633–639

Gatta GD, Boffa Ballaran T, Comodi P, Zanazzi PF (2004b) Comparative compressibility and equation of state of orthorhombic

and tetragonal edingtonite. Phys Chem Miner 31:288–298
Gottardi G, Galli E (1985) Natural zeolites. Springer-Verlag, Berlin, D, p 409
Hazen RM, Finger LW (1982) Comparative crystal chemistry. Wiley, New York, USA
Heinz DL, Jeanloz R (1984) The equation of state of the gold calibration standard. J Appl Phys 55:885–893
Larson AC, Von Dreele RB (2004) General structure analysis system (GSAS), Los alamos national laboratory report LAUR, pp 86–748
Le Bail A, Duroy H, Fourquet JL (1988) Ab-initio structure determination of $LiSbWO_6$ by X-ray powder diffraction. Mat Res Bull 23:447–452
Lee Y, Vogt T, Hriljac JA, Parise JB, Artioli G (2002a) Pressure-induced volume expansion of zeolites in the natrolite family. J Am Chem Soc 124:5466–5475
Lee Y, Vogt T, Hriljac JA, Parise JB, Hanson JC, Kimk SJ (2002b) Non-framework cation migration and irreversible pressure-induced hydration in a zeolite. Nature 420:485–489
Lee Y, Hriljac JA, Studer A, Vogt T (2004) Anisotropic compression of edingtonite and thomsonite to 6 GPa at room temperature. Phys Chem Miner 31:22–27
Lemonnier M, Fourme R, Rosseaux F, Kahn R (1978) X-ray curved-crystal monochromator system at the storage ring DCI. Nucl Instrum Methods 152:173–177
Mao HK, Xu J, Bell PM (1986) Calibration of the ruby pressure gauge to 800 kbar under quasi-hydrostatic conditions. J Geophys Res 91:4673–4676
Martucci A, Sacerdoti M, Cruciani G, Dalconi C. (2003) In situ time resolved synchrotron powder diffraction study of mordente. Eur J Miner 15:485–493
Meier WM (1961) The crystal structure of mordenite. Z Kristallogr 115:439–450
Miletich R, Allan DR, Kush WF (2000) High-pressure single-crystal techniques. In: Hazen RM, Downs RT (eds) High-temperature and high-pressure crystal chemistry. Reviews in mineralogy and geochemistry, vol 41. Mineralogical Society of America and Geochemical Society, Washington, DC, pp 445–519
Mortier WJ, Pluth JJ, Smith JV (1975) Positions of cations and molecules in zeolites with the mordenite-type framework. I. Dehydrated Ca-exchanged ''ptilolite''. Mat Res Bull 10:1037–1046
Mortier WJ, Pluth JJ, Smith JV (1976) Positions of cations and-molecules in zeolites with the mordenite-typeframework. III. Rehydrated Ca-exchanged ptilolite. Mat Res Bull 11:15–22
Ohashi Y (1982) STRAIN: a program to calculate the strain tensor from two sets of unit-cell parameters. In: Hazen RM, Finger LW (eds) Comparative crystal chemistry. Wiley, New York, pp 92–102
Passaglia E, Sheppard RA (2001) The crystal chemistry of zeolites. In: Bish DL, Ming DW (eds) Natural zeolites: occurrence, properties, application. Reviews in mineralogy and geochemistry, vol 45. Mineralogical Society of America and Geochemical Society, Washington, DC, pp 69–116
Rietveld HM (1969) A profile refinement method for nuclear and magnetic structures. J Appl Crystallogr 2:65–71
Schlenker JL, Pluth JJ, Smith JV (1978a) Positions of cations and molecules in zeolites with themordenite-typeframework.V. Dehydrated Rb-mordenite. Mat Res Bull 13:77–82
Schlenker JL, Pluth JJ, Smith JV (1978b) Positions of cations and molecules in zeolites with the mordenite-type framework. VI. Dehydrated barium mordenite. Mat Res Bull 13:169–174
Schlenker JL, Pluth JJ, Smith JV (1978c) Positions of cations and molecules in zeolites with the mordenite-type framework. VII. Dehydrated cesium mordenite. Mat Res Bull 13:901–905
Schlenker JL, Pluth JJ, Smith JV (1979) Positions of cations and-molecules in zeolites with the mordenite-type framework.VIII. Dehydratedsodium-exchanged mordenite. Mat Res Bull 14:751–758
Simoncic P, Armbruster T (2004) Peculiarity and defect structure of the natural and synthetic zeolite mordenite: a single-crystal X-ray study. Am Miner 89:421–431
Smith GC (1991) X-ray imaging with gas proportional detectors. Synch. Rad. News 4:24–30
Thomson P, Cox DE, Hastings JB (1987) Rietveld refinement of Debye-Scherrer synchrotron X-ray data from Al_2O_3. J Appl Crystallogr 20:79–83